Tirhert and Aouinet Legraa: Rare unbrecciated eucrite falls

Taha Shisseh, Hasnaa Chennaoui Aoudjehane, Carl Agee, Omar Boudouma

The Meteoritical Society

Meteoritics & Planetary Science 57, Nr 10, 1920–1935 (2022)
doi: 10.1111/maps.13899

Tirhert and Aouinet Legraa: Rare unbrecciated eucrite falls

Taha SHISSEH[1]*, Hasnaa CHENNAOUI AOUDJEHANE[1], Carl B. AGEE[2], and Omar BOUDOUMA[3]

[1]GAIA Laboratory, Faculty of Sciences Ain Chock, Hassan II University of Casablanca, km 8 Route d'El Jadida, 20150 Casablanca, Morocco
[2]Institute of Meteoritics, University of New Mexico, Albuquerque, New Mexico 87131, USA
[3]UPMC – Paris 06, UMR, 7193 Paris, France
*Corresponding author. E-mail: shisseh.taha1@gmail.com

(Received 13 November 2021; revision accepted 27 June 2022)

Abstract–Tirhert and Aouinet Legraa are the only documented unbrecciated eucrite falls in Africa. Aouinet Legraa fell in Algeria on July 17, 2013. Tirhert's fall occurred about a year later in Morocco, on July 9, 2014. Both meteorites are covered by a black and glossy fusion crust as is typical of eucrites. Tirhert has a poikilitic texture with remnant subophitic pockets, and consists of millimeter-sized grains of plagioclase (An_{87-91}), pigeonite (Mg# 42) with augite exsolution lamellae, and interstitial opaque minerals. Aouinet Legraa has a subophitic texture, and it is dominated by plagioclase laths (An_{82-89}) enclosed by pigeonite (Mg# 37), with exsolution lamellae of augite. Remnant Ca zoning in pyroxene is observed in both rocks, although it is more abundant in Aouinet Legraa than Tirhert. The presence of exsolved pyroxenes suggests that these meteorites have undergone thermal metamorphism. Equilibration temperatures estimated from pigeonite and augite pairs using the QUILF program are ~931 °C in Tirhert and ~758 °C in Aouinet Legraa. This indicates that these rocks had distinct thermal histories. Aouinet Legraa has trace element abundances similar to the typical main group eucrite Juvinas, confirming its origin as a main group eucrite. The trace element abundances of Tirhert fall between those of cumulate and main group eucrites. Its rare earth element pattern is flat with a positive Eu anomaly. This likely suggests that Tirhert is a partial cumulate of plagioclase from a main group magma, or a flotation cumulate formed by flotation of plagioclase in a subvolcanic chamber or by scavenging crystals during eruption.

INTRODUCTION

The meteorites of the howardite–eucrite–diogenite suite (HED) are the most abundant achondritic class in the world meteorite collection. As of June 20, 2021, 2421 HED meteorites have been recovered from the Earth's surface (www.lpi.usra.edu/meteor/metbull.php). Eucrites are basaltic and gabbroic rocks formed in the upper crust of their parent body. Diogenites are lower crustal samples composed predominantly of orthopyroxenes. Howardites are regolith breccias composed mainly of eucritic and diogenitic fragments (Mittlefehldt, 2015). The crystallization age of these achondrites suggests that their parent body was accreted and differentiated within the first 1–4 Ma of solar system formation (Connelly et al., 2017; Kleine et al., 2009; Kleine & Wadhwa, 2017; Neumann et al., 2014; Touboul et al., 2015) and that magmatic activity may have lasted over a period of 35–50 Ma (Roszjar et al., 2016; Zhou et al., 2013).

It is generally accepted that the 525 km asteroid (4) Vesta and its dynamically associated family (i.e., the Vestoids) are the sources of the HED meteorites (Binzel & Xu, 1993; Burbine et al., 2001; De Sanctis et al., 2013; McSween et al., 2013). Vesta had an intense collisional history, as evidenced by the discovery of a large number of impact craters on its surface (Marchi et al., 2012; McCoy et al., 2015; Williams et al., 2014). The southern hemisphere of Vesta contains two overlapping impact basins named Rheasilvia (500 ± 25 km in diameter) and

Veneneia (400 ± 20 km in diameter; Marchi et al., 2012). The excavated material from Rheasilvia alone could account for the entire mass of vestoids and HED material reaching Earth (Russell et al., 2012). Some authors speculate that Vesta is not the parent body of howardites, diogenites, and eucrites. Wasson (2013) compared the Cr and O isotopic compositions of IIIAB and HED meteorites and suggested that the latter originated from the IIIAB parent body and not Vesta. Mg-isotopic data showed that the parent body of diogenites completely melted and solidified within 2–3 Myr (Schiller et al., 2011). This rapid formation could only occur on bodies less than 100 km in diameter. If this is true, it could be suggested that Vesta is not the parent body of the HED meteorites.

Most eucrites experienced thermal metamorphism, as evidenced by their textures, mineralogies, and compositions (Mayne et al., 2009; Takeda & Graham, 1991; Yamaguchi et al., 1996, 1997, 2009). Takeda and Graham (1991) divided eucrites into six types based on the degree of equilibration of their pyroxenes, with type 1–2 being the least metamorphosed and type 6 the most metamorphosed. Type 7 was introduced by Yamaguchi et al. (1996) for eucrites that exhibit features of both type 4 (residual Ca-zoning) and type 6 (inversion of pigeonite). Other effects of thermal metamorphism include inclusions in the major mineral phases of basaltic eucrites, giving them a cloudy appearance (Harlow & Klimentidis, 1980; Schwartz & McCallum, 2005).

Eucrites are subdivided into noncumulates, restites, and cumulates based on the concentrations of their major and trace elements (Barrat et al., 2007; Stolper, 1977; Yamaguchi et al., 2009). Three groups of noncumulate eucrites are distinguished: (1) the main group eucrites with moderate Mg# and incompatible element abundances; (2) the Nuevo Laredo group with compositions that are consistent with a simple pyroxene fractionation from the main group—with lower Mg#s (more ferroan) and abundances of compatible elements and correlated enrichments in igneous incompatible elements; (3) the Stannern group with incompatible element-rich compositions and similar Mg# values to the main group eucrites. Restites (i.e., residual eucrites) are formed through partial melting of some of the most metamorphosed main group eucrites and are characterized by positive Eu anomalies and LREE depletions (Yamaguchi et al., 2009). Cumulate eucrites have lower abundances of incompatible elements, and their REE patterns display a positive Eu anomaly consistent with their formation by accumulation of plagioclase (Mittlefehldt & Lindstrom, 1993).

This paper focuses on the mineralogy, petrography, and geochemistry of the unbrecciated eucrites Tirhert and Aouinet Legraa. These meteorites are fresh fall meteorites, and so have not experienced any terrestrial weathering, physical or chemical. Therefore, they have preserved their original magmatic composition before and after their ejection from the asteroid Vesta. Unbrecciated eucrites are rare and represent only a small fraction (~11%) of the total HED meteorites. They are considered the most suitable lithology for building and testing models of crust formation and evolution. This is in contrast to brecciated eucrites, which generally contain a mixture of endogenous (cumulative, basaltic, and diogenitic; Mittlefehldt, 2015) and exogenous (Fe-Ni metal, chondritic, and achondritic; Lorenz et al., 2007) materials, as well as shock features that make it difficult to constrain their original composition.

METHODS

To gather further information from eyewitnesses, a field mission was organized to Foum El Hisn (Southern Morocco), near the Tirhert fall site. The following members participated in this expedition: Hasnaa Chennaoui Aoudjehane, Mohamed Aoudjehane, Ahmed Bouferra, Ahmed Bouragaa, and Adam Aaranson. The data collected include a detailed description of the meteoroid entry (date, time, duration, direction, trajectory), the associated phenomena (light intensity and color, fragmentation, sonic booms), as well as the number of pieces recovered, their physical properties, mass, and coordinates (see Table S1 in the supporting information).

Two polished sections from Tirhert and Aouinet Legraa were prepared for optical and scanning electron microscope (SEM)/back-scattered electron (BSE) petrographic study and electron probe microanalysis (EPMA) chemical analyses. Microscopic images were acquired using a Zeiss SUPRA 55-VP FEGSEM scanning electron microscope equipped with a Bruker QUAD EDS detector at the "Institut des Sciences de la Terre de Paris" (ISTeP), Sorbonne University, France, in BSE mode at an accelerating voltage of 15 kV. A total of 55 energy-dispersive X-ray spectroscopy (EDS) elemental maps were also obtained using the same system. The chemical composition of the major and minor mineral phases (pyroxene, plagioclase, silica, and oxides) was determined using a CAMECA SX-FIVE EPMA at ISTeP, Sorbonne University, France, at an accelerating voltage of 15 kV and a beam current of 10 nA. The following standards were used for calibration: orthose (Al, K), apatite (P), pyrite (Fe), NiO (Ni), ZrSi (Zr), Cr_2O_3 (Cr), albite (Na), diopside (Mg, Si, Ca), $MnTiO_3$ (Ti, Mn). The trace element concentrations were obtained using 1 g of Tirhert and 1 g of Aouinet Legraa. Analyses

were performed by inductively coupled plasma-sector field mass spectrometry using a Thermo Element 2 spectrometer at Institut Universitaire Européen de la Mer (IUEM), Plouzané, following the procedures described in Barrat et al. (2016). The rare earth element (REE) concentrations were normalized to the concentrations of CI listed in the work of Barrat et al. (2012). Silica polymorphs were investigated using inVia Renishaw Raman microscope equipped with 532 and 785 nm laser sources at the "Centre de Recherche sur la Conservation" (CRCC), Museum National d'Histoire Naturelle Paris, France. Fiji-ImageJ and Adobe Photoshop were used to process the SEM images, create colored images, and estimate the modal abundances of the minerals (see the supporting information). To estimate the equilibration temperatures of pyroxene, we used the QUILF (quartz–ulvöspinel–ilmenite–fayalite) program (Andersen et al., 1993).

TIRHERT

Fall History

The fall of Tirhert occurred on July 9, 2014, at 9:30 pm GMT. Eyewitnesses from Douar El Mougadir (Foum El Hisn), the village of Tirhert and locations 220 km from the fall site reported a strong fireball crossing the sky horizontally in a NW–SE direction and lasting for about 4 s. The light was strong and had a white to yellow color that later changed to red and blue. The meteoroid experienced several explosions during its entry into the atmosphere, producing a shower of luminous pieces followed by three sonic booms. A few witnesses reported hearing a whistling sound at the same time as the fireball. Thousands of people from nearby villages began searching for the debris. The first pieces were found the next day between Foum El Hisn and Tirhert (Figs. S1 and S2 in supporting information). Using the geographic coordinates of many finders, we constructed a strewn field of 6 × 3 km, which we plotted on the Moroccan topographic map Talrhaicht (Fig. 1; see Table S2 in supporting information). A total weight of 8–10 kg was recovered (Table S2) (Ruzicka et al., 2017). Note that the Tirhert fall site is located 140 km from the fall site of the famous Martian meteorite Tissint, 174 km from the fall site Sidi Ali Ou Azza, and only 49 km from the fall site Kheneg Ljouâd (Chennaoui Aoudjehane et al., 2012, 2016; Chennaoui Aoudjehane & Garvie, 2018).

Macroscopic Description

Most fragments of Tirhert are covered by a shiny black fusion crust typical of eucrites. Grains of

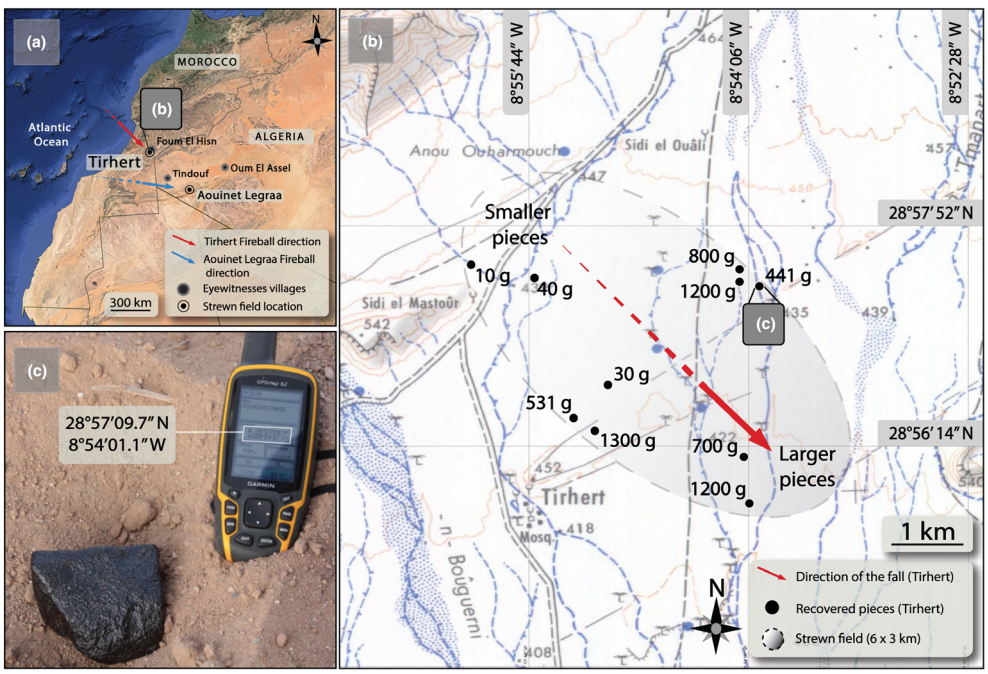

Fig. 1. a) Tirhert and Aouinet Legraa fireball trajectories and fall locations. The red arrow is showing the fireball direction of Tirhert, which has been constructed using information provided by eyewitnesses. Blue arrow is Aouinet Legraa fireball trajectory. b) Close-up view of Tirhert fall site. The largest pieces (up to 1300 g in weight) are found in the southern part of the fall area, whereas small fragments were recovered from the northern side. c) Tirhert specimen (441 g) and its geographic coordinates. Note the shiny fusion crust as is typical of eucrites. (Color figure can be viewed at wileyonlinelibrary.com.)

plagioclase and pyroxene are found scattered in the melted surface (Fig. 2a and 2b; Fig. S2b). The interior is friable and dominated by coarse, subrounded to rounded grains of white plagioclase, honey-brown pyroxene, and small opaques (Fig. 2b; Fig. S2c). No shock veins or melting features were encountered.

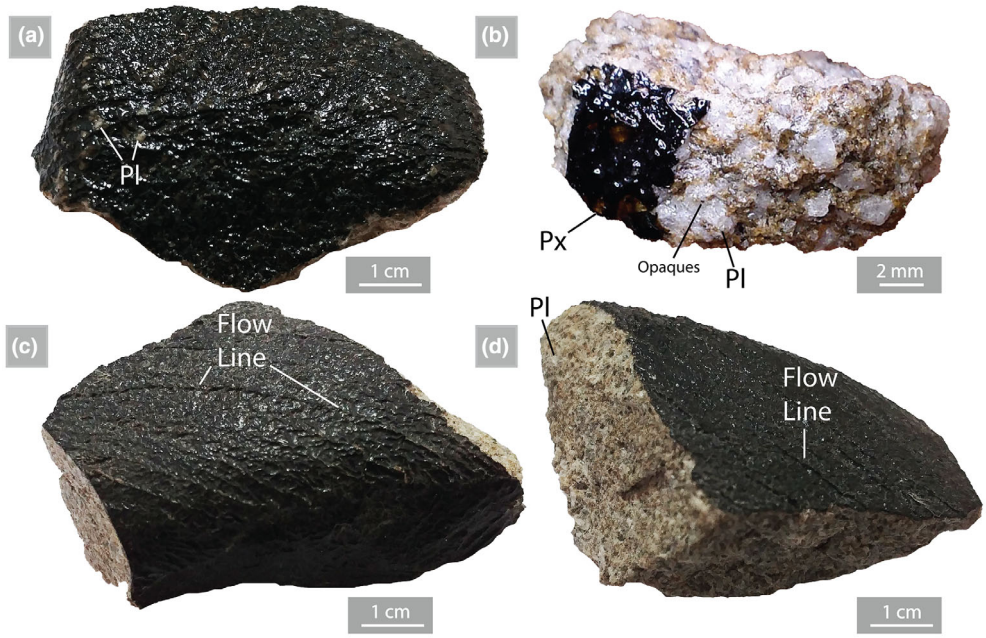

Fig. 2. Macroscopic photos of Tirhert and Aouinet Legraa. a) The fusion crust in Tirhert is shiny and contains discontinuous flow lines and ridges. Note the presence of pyroxene and plagioclase grains beneath the surface. b) Holocrystalline texture of Tirhert. White grains are plagioclase, brown grains are pyroxene and tiny black grains are opaques. c) Well-developed flow lines running down the side of Aouinet Legraa. d) The interior of Aouinet Legraa is mostly dominated by plagioclase laths enclosed by brown pyroxene. (Color figure can be viewed at wileyonlinelibrary.com.)

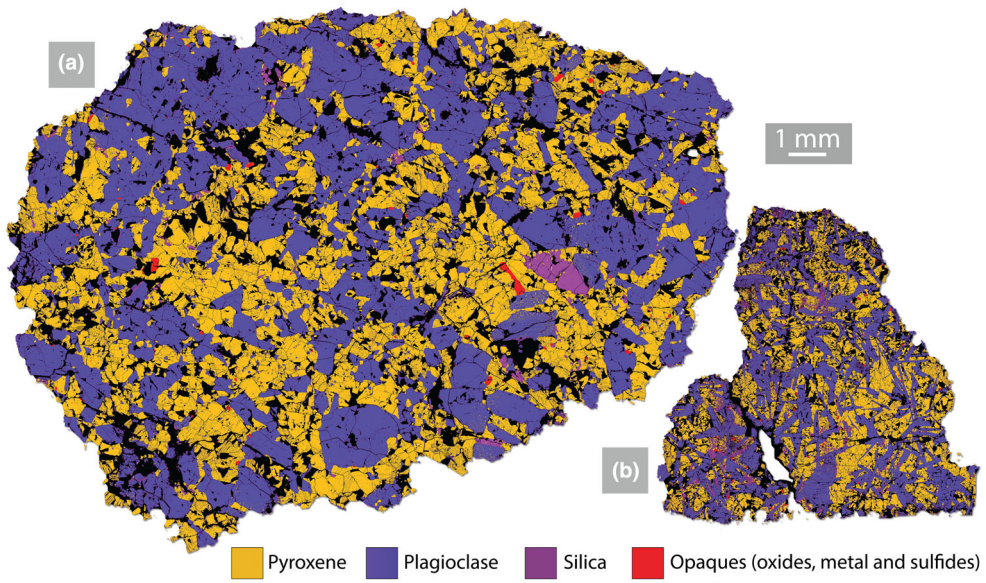

Fig. 3. Colored mosaic images showing the textural characteristics of Tirhert and Aouinet Legraa. a) Tirhert has a poikilitic texture with 2-mm-sized pyroxene and plagioclase. Silica and oxides are rare and mostly occur between major mineral boundaries. b) Aouinet Legraa exhibits a subophitic texture. Silica (purple) is mostly found enclosed between plagioclase laths. Note the high abundance of oxides (mainly ilmenite). (Color figure can be viewed at wileyonlinelibrary.com.)

Mineralogy

Tirhert is 49.5% plagioclase, 28% low-Ca pyroxene, 19.5% high-Ca pyroxene, 2.5% silica, and 0.5% opaques (Fig. 3; Fig. S6 and Table S3 in supporting information). This meteorite has a poikilitic texture and consists of equal-sized subhedral to anhedral plagioclase and pyroxene (~1 to 2 mm). The fusion crust is between 50 and 100 μm thick and includes mineral fragments and vesicles (10–40 μm in diameter; Fig. S3a in supporting information). Some areas of the thin section show remnants of subophitic textures (Fig. S3b). Pyroxene is predominantly pigeonite, but occasional grains of augite were also detected. Most of the pigeonite contains parallel, 1 μm thick exsolution lamellae of augite, spaced about 4 μm apart (Fig. 4). Common, well-developed augite lamellae up to 40 μm wide are also observed in pigeonite. In some cases, pyroxene displays remnant Ca-zoning (Fig. 4a; Fig. S4 in supporting information). Plagioclase blebs, tiny ilmenite, and chromite grains occur as scattered inclusions in pyroxene (Fig. 4a; Fig. S4). Plagioclase is generally not cloudy, but some grains contain rods and blebs of high- and low-Ca pyroxene, as well as silica and troilite inclusions that follow crystallographic directions (Fig. 4a). Mesostasis is nearly absent in Tirhert, except for an area that has residual subophitic texture and consists of subhedral silica grains and troilite inclusions (Fig. S3b).

Minor phases include silica, chromite, ulvöspinel, ilmenite, troilite, phosphates, and zircon. They usually occur in contact with pyroxene and plagioclase or as inclusions in the main minerals, giving them a cloudy appearance. A single anhedral silica grain (1 × 0.5 mm) with inclusions was discovered near extremely clouded pyroxene and plagioclase (Fig. 4a; Fig. S4a). Subhedral to anhedral opaques (chromite, ulvöspinel, and ilmenite) range in size from a few micrometers to 200 μm. The oxide grain in Fig. 4a (500 × 100 μm) is closely associated with ilmenite and occurs in proximity to pyroxene with remnant Ca-zoning (Fig. S4a). Chromite grains often contain exsolved ilmenite lamellae (50 μm thick) associated with troilite (Fig. 4b). Accessory phases such as zircon are generally 40 μm in size and occur spatially in close proximity to plagioclase, chromite, and ilmenite grains (see Fig. S4).

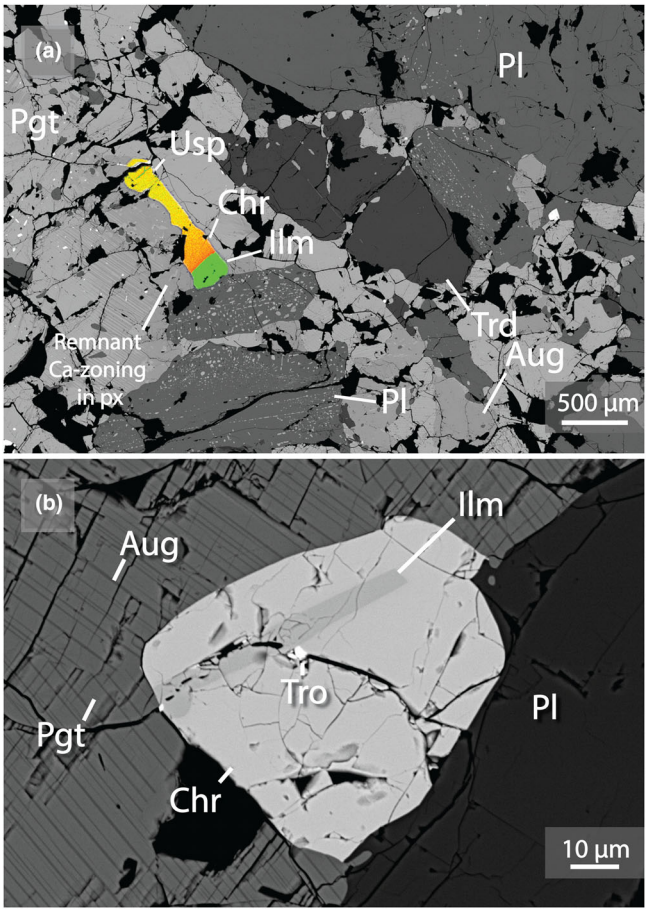

Fig. 4. Backscattered electron images (BSE) of Tirhert. a) Tirhert mainly consists of plagioclase and pyroxene. Plagioclase is mostly clear, but few crystals contain abundant low- and high-Ca pyroxene, silica and troilite inclusions. Silica grain the center of the image is monoclinic tridymite. Note the remnant Ca-zoning in pyroxene in close vicinity of the oxide grain, which has ulvöspinel, chromite and ilmenite compositions as shown by the superimposed false-colored EDS elemental map (red = Cr, green = Ti; the full EDS maps are given in Fig. S4a in supporting information). b) Chromite with ilmenite exsolution lamellae and troilite. Pgt = pigeonite; Aug = augite; Pl = plagioclase; Trd = tridymite; Usp = ulvöspinel; Chr = chromite; Ilm = ilmenite; Tro = troilite. (Color figure can be viewed at wileyonlinelibrary.com.)

Mineral Compositions

The average composition of pyroxene in Tirhert is given in Table 1. The pyroxene endmember compositions and minor element (Al, Ti, Cr) are plotted in Fig. 5a. The average Fe/Mn ratios in pyroxene from Tirhert are ~31, which is in the range of basaltic eucrites (Fig. S7 in supporting information). The Fe and Mg contents in Tirhert's pyroxene are homogenized. Figure 5a shows that the compositions of pyroxene are following the Fe-Ca trend, consistent with mixing between the compositions of the host pigeonite and exsolved augite, implying that host and exsolution lamellae were included in the analytical volumes. The average composition of low-Ca pyroxene is $En_{38\pm1.19}Fs_{53\pm3.9}Wo_{9\pm4.5}$ (n = 16; Mg# = 42). Augite exsolution lamellae are $En_{31\pm1.2}Fs_{32\pm3.9}Wo_{37\pm4.8}$ (n = 19). Pyroxene with remnant Ca-zoning is $En_{38}Fs_{57}Wo_5$ in the core and becomes $En_{36}Fs_{45}Wo_{17}$

Table 1. Average EPMA data (wt%) of low- and high-Ca pyroxene in Tirhert and Aouinet Legraa.

	Tirhert		Aouinet Legraa		Aouinet Legraa (mesostasis)
	Low-Ca pyroxene (n = 17)	High-Ca pyroxene (n = 17)	Low-Ca pyroxene (n = 9)	High-Ca pyroxene (n = 7)	High-Ca pyroxene (n = 2)
SiO_2	48.87	50.15	50.21	50.68	50.75
MgO	12.58	10.46	11.50	9.44	10.50
Al_2O_3	0.32	0.72	0.20	0.62	0.51
P_2O_5	0.02	0.29	n.d.	0.31	0.22
K_2O	0.01	n.d.	0.01	0.01	n.d.
CaO	3.23	19.03	2.81	19.14	19.24
TiO_2	0.40	0.97	0.22	0.66	0.36
FeO	32.17	16.99	34.29	17.95	18.86
NiO	0.02	n.d.	0.03	0.11	n.d.
Cr_2O_3	0.21	0.29	0.12	0.30	0.22
MnO	1.02	0.35	1.04	0.53	0.51
ZrO_2	n.d.	n.d.	n.d.	n.d.	n.d.
Total	99	99.47	100.53	99.88	99.20
En	37.91 ± 1.21	32.63 ± 3.7	35.1 ± 0.3	29. 14 ± 0.4	29.29 ± 0.22
Fs	52.75 ± 4	30.38 ± 7.9	58.9 ± 0.5	30.07 ± 0.35	29.94 ± 0.62
Wo	9.34 ± 4.5	36.98 ± 6	6 ± 0.4	40.79 ± 0.5	40.76 ± 0.8
Fe/Mn	31.06	47.49	32.55	33.70	36.34
Fe/Mg	1.43	0.91	1.67	1.07	1.01

n.d. = not detected.

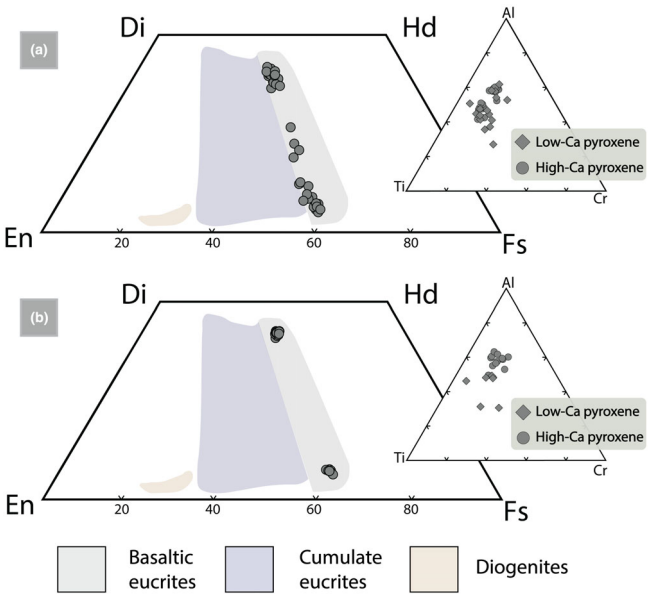

Fig. 5. Pyroxene end-member compositions in Tirhert (a) and Aouinet Legraa (b). Minor element contents (Cr, Ti, Al) of low- and high-Ca pyroxene are also plotted. Intermediate compositions between low- and high-Ca pyroxene in Tirhert are due to EPMA beam overlap. Compositional fields of pyroxene from diogenites, cumulate eucrites and basaltic eucrites are from Yamaguchi et al. (2017) and references therein. (Color figure can be viewed at wileyonlinelibrary.com.)

then $En_{32}Fs_{32}Wo_{36}$ toward the rim. The pyroxene inclusions in plagioclase in Tirhert are similar in composition to the pyroxene of the host igneous pyroxene ($En_{39}Fs_{52}Wo_9$). Mayne et al. (2009) showed that the major and minor elements of eucritic pyroxene do not equilibrate at the same temperatures. Metamorphosed eucrites can contain pyroxene with equilibrated major element compositions (Fe-Mg-Ca), but still exhibit zoning with respect to their minor element content (Al-Ti-Cr). Minor elements in Tirhert's pyroxene are homogeneous to some extent, with nearly constant Cr and a little variation of Ti and Al (Fig. 5a).

The EPMA data of plagioclase in Tirhert are presented in Table 2. The plagioclase endmember compositions are plotted in Fig. 6a. The compositions range from An_{87} to An_{91}. Plagioclase inclusions in pyroxene do not have unusual compositions and are comparable to those measured in igneous plagioclase (see Table 2). K (afu) versus An (%) of plagioclase in Tirhert are plotted in Fig. S8 in supporting information, along with data from diogenites, basaltic, and cumulate eucrites. These values plot within the range of HED meteorites (Consolmagno et al., 2015; Papike, 1998).

Minor and accessory phases include silica, chromite, ulvöspinel, ilmenite, troilite, phosphates, and zircon (see Table S4 for EPMA data of zircon). Electron microprobe data of spinel (chromite and ulvöspinel) and ilmenite are given in Table 3. The compositions of chromite and ulvöspinel are plotted in Fig. 7. The silica phase is tridymite (98.14 ± 0.3 wt%; Table 4), as determined by Raman spectroscopy (see Fig. S9 in supporting information). Chromite and ulvöspinel occur in Tirhert in contact with pyroxene and plagioclase or

Table 2. Average analyses (wt%) of plagioclase and plagioclase inclusions within clouded pyroxene in Tirhert and Aouinet Legraa.

	Plagioclase		Plagioclase (inclusions in pyroxene)	
	Tirhert (n = 5)	Aouinet Legraa (n = 8)	Tirhert (n = 1)	Aouinet Legraa (n = 1)
SiO_2	45.72	46.48	45.71	45.35
MgO	0.04	n.d.	n.d.	0.02
Al_2O_3	34.73	34.68	35.02	34.41
Na_2O	1.07	1.5	1.09	1.29
P_2O_5	0.17	0.24	0.26	0.1
K_2O	0.09	0.1	0.06	0.1
CaO	17.79	17.92	17.78	17.57
TiO_2	0.02	n.d.	n.d.	n.d.
FeO	0.39	0.02	0.79	0.98
NiO	n.d.	n.d.	n.d.	0.01
Cr_2O_3	n.d.	n.d.	n.d.	n.d.
MnO	0.03	0.02	0.07	0.05
ZrO_2	n.d.	n.d.	n.d.	0.1
Total	100.05	100.96	100.98	99.76
An	89.44 ± 1.65	88.28 ± 1.2	88.05	89.41
Ab	10.04 ± 1.74	11.14 ± 1.2	11.57	10
Or	0.52 ± 0.13	0.58 ± 0.1	0.38	0.59

n.d. = not detected.

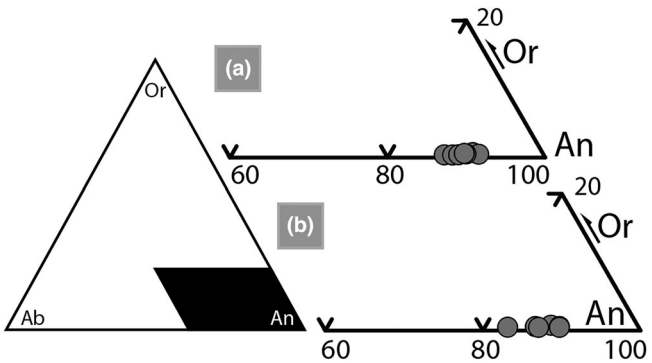

Fig. 6. Plagioclase end-member compositions in Tirhert (a) and Aouinet Legraa (b).

interstitial to pyroxene. Compositions range up to $Chr_{62}Usp_{26}$ and $Chr_{34}Usp_{63}$. The oxide grain (500 × 100 μm) shown in Fig. 4a consists of chromite ($Chr_{53}Spl_{11}$), ulvöspinel ($Usp_{57}Spl_8$), and ilmenite with ~0.1 wt% Cr_2O_3, 1.3 wt% MgO, and 0.8 wt% MnO. The composition of the grain (Fig. 4b) with exsolved ilmenite lamellae (up to 8 μm wide) is $Chr_{45}Usp_{44}$ and becomes more enriched in Ti toward the lamellae ($Chr_{38.3}Usp_{52.7}$). Ilmenite exhibits a homogeneous composition with FeO and TiO_2 contents of 44 and 51 wt%, respectively. These values are consistent with the composition of ilmenite in basaltic eucrites (Mayne et al., 2009; Mittlefehldt, 2015).

Trace and Rare Element Composition

The bulk composition of Tirhert is given in Table 5. The CI-normalized REE pattern of this meteorite is plotted in Fig. 8, together with REE patterns of the main group eucrite Juvinas, the residual eucrites Agoult and DaG 945, the Stannern eucrite Bouvante, the eucrite Nuevo Laredo, the partial cumulate Pomozdino, and the cumulate eucrites Y-791195 and Moore County (Barrat et al., 2007; Barrett et al., 2017; Mittlefehldt & Lindstrom, 1993; Warren et al., 1990, 2009; Yamaguchi et al., 2009). Tirhert's previously reported REE values are also plotted for comparison (Barrett et al., 2017).

The REE pattern of Tirhert is about ~8–9 × CI, and displays a pronounced positive Eu anomaly (Eu/Eu* = 1.26; Fig. 8). Trace elements such as Sc, La, and Hf can be used as tools to distinguish between different geochemical groups of basaltic eucrites. Scandium is relatively compatible in pyroxene and incompatible in plagioclase, while La and Hf are incompatible in both pyroxene and plagioclase (Mittlefehldt & Lindstrom [1993] and references therein); these elements are commonly used to distinguish the geochemical groups of eucrites. Our data show that Tirhert plots between the fields of main group and cumulate eucrites, as it contains lower abundances of Sc, La, and Hf than the main group (Fig. 9).

AOUINET LEGRAA

Fall History

On July 17, 2013, a bright fireball was observed near Tindouf and western Algeria, moving in an eastern direction. The event was also reported by residents of the village Oum El Assel. Witnesses stated that no sonic boom was heard. Local hunters began searching for debris immediately after the event. It took 9 months, until April 2014, to find the exact fall site (Fig. 1a). The total weight recovered was estimated at 58 kg (Bouvier et al., 2017).

Macroscopic Description

The fusion crust of Aouinet Legraa consists of ridges and flow lines running along the side of the rock. These features formed naturally during an oriented atmospheric entry of the meteoroid (Fig. 2c and 2d). The interior of the rock has a spongy appearance because it is interbedded with white, millimeter-sized plagioclase lamellae that trap pyroxenes and brown sulfides.

Table 3. Representative average analyses (wt%) of spinel (chromite and ulvöspinel) and ilmenite in Tirhert and Aouinet Legraa.

	Chromite		Ulvöspinel		Ilmenite	
	Tirhert (n = 3)	Aouinet Legraa (n = 1)	Tirhert (n = 11)	Aouinet Legraa (n = 3)	Tirhert (n = 2)	Aouinet Legraa (n = 1)
SiO_2	0.02	0.06	n.d.	n.d.	0.05	0.04
MgO	1.28	0.78	1.00	0.98	1.69	1.23
Al_2O_3	5.64	7.33	3.52	3.92	n.d.	n.d.
Na_2O	n.d.	n.d.	0.03	0.16	0.04	n.d.
P_2O_5	n.d.	0.04	n.d.	0.10	n.d.	n.d.
K_2O	n.d.	n.d.	n.d.	n.d.	n.d.	n.d.
CaO	n.d.	0.12	0.02	0.04	0.02	0.06
TiO_2	12.59	8.60	22.62	24.86	51.11	52.15
FeO	42.44	39.53	48.28	38.89	44.00	44.80
NiO	n.d.	n.d.	0.04	0.02	n.d.	n.d.
Cr_2O_3	36.89	40.11	24.61	29.62	0.16	0.22
MnO	0.49	0.45	0.25	0.23	0.80	0.83
ZrO_2	0.05	n.d.	n.d.	0.07	0.07	n.d.
Total	100	98.06	100.38	98.89	98.00	99.38
Usp	37.17 ± 9.5	23.81	57.31 ± 5.8	56.69 ± 11		
Spl	11.83 ± 2.15	15.90	8.41 ± 0.79	8.4 ± 0.25		
Chr	53.68 ± 8.9	58.37	38. 27 ± 2.8	40.91 ± 2.39		

n.d. = not detected.

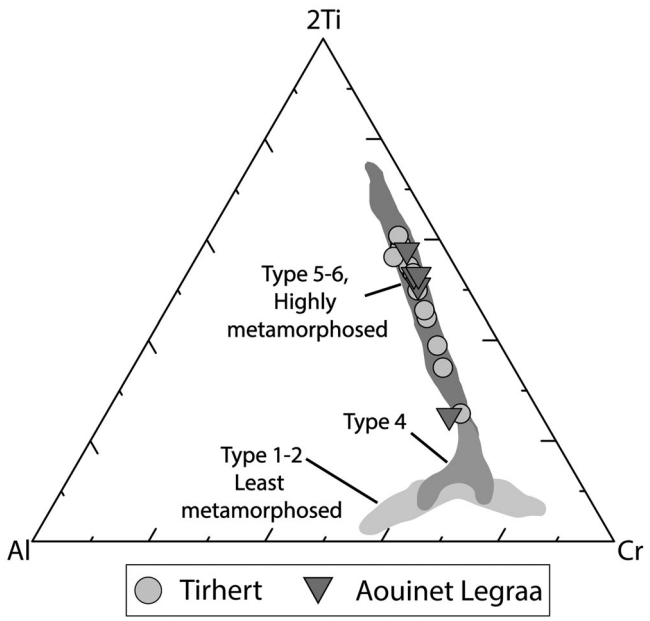

Fig. 7. Chromite and ulvöspinel compositions in Tirhert and Aouinet Legraa. Metamorphic ranges are taken from Yamaguchi (2000).

Table 4. Representative EPMA analysis of silica in Tirhert and Aouinet Legraa.

	Silica		Mesostasis silica	
	Tirhert (n = 5)	Aouinet Legraa (n = 2)	Tirhert (n = 1)	Aouinet Legraa (n = 2)
SiO_2	98.50	100.04	99.51	98.53
MgO	n.d.	0.03	n.d.	n.d.
Al_2O_3	0.44	0.27	0.20	0.22
Na_2O	n.d.	n.d.	0.02	0.04
P_2O_5	0.03	n.d.	n.d.	0.02
K_2O	0.23	0.16	0.14	0.14
CaO	0.01	0.02	0.05	0.01
TiO_2	0.17	0.04	0.10	0.07
FeO	0.04	0.17	0.30	0.24
NiO	0.03	n.d.	n.d.	n.d.
Cr_2O_3	n.d.	n.d.	0.05	0.02
MnO	n.d.	n.d.	0.03	n.d.
ZrO_2	n.d.	n.d.	n.d.	0.14
Total	99.44	100.73	100.42	99.56

n.d. = not detected.

Mineralogy

Aouinet Legraa consists of 45.5% plagioclase, 51% pyroxene, 3% silica, and 0.5% opaques (Fig. 3; Fig. S6 and Table S3). This rock exhibits a subophitic texture with interconnected, extremely clouded, and fractured plagioclase grains, up to 1–2 mm long but only 50–100 μm wide. The host pigeonite is generally exsolved and contains high-Ca pyroxene exsolution lamellae up to 40 μm wide (Fig. 10a; see also Fig. S5 in supporting information). Pyroxene with remnant Ca-zoning is abundant, and mostly occurs in the vicinity of mesostasis. Pigeonite exsolution lamellae (10 μm thick) occur in several augite grains. Cracks in pyroxene are commonly filled with discontinuous rods and lenses of 20 μm plagioclase, silica, and chromite

Table 5. Trace element compositions of Tirhert and Aouinet Legraa. Oxides are in wt% and trace elements in μg g^{-1}.

	Tirhert	Aouinet Legraa		Tirhert	Aouinet Legraa		Tirhert	Aouinet Legraa
TiO_2	0.45	0.62	Sr	77.21	74.95	Tb	0.32	0.40
P_2O_5	0.01	0.03	Y	13.85	17.08	Dy	2.18	2.72
Be	0.08	0.14	Zr	27.59	39.60	Ho	0.49	0.60
K	270.21	318.41	Nb	1.75	2.85	Er	1.42	1.74
Sc	28.09	30.82	Ba	25.61	28.47	Yb	1.40	1.66
V	67.54	63.11	La	1.98	2.52	Lu	0.21	0.24
Mn	4013.82	3803.79	Ce	5.04	6.46	Hf	0.80	1.13
Co	5.80	5.04	Pr	0.77	0.99	Ta	0.11	0.16
Cu	—	0.50	Nd	3.86	4.98	W	0.03	0.06
Zn	—	1.06	Sm	1.26	1.61	Pb	—	0.06
Ga	1.52	1.46	Eu	0.61	0.62	Th	0.25	0.31
Rb	0.11	0.20	Gd	1.73	2.21	U	0.06	0.08
Eu/Eu*	1.26	0.99	Hf/Sm	0.64	0.70	Th/U	4.04	4.06

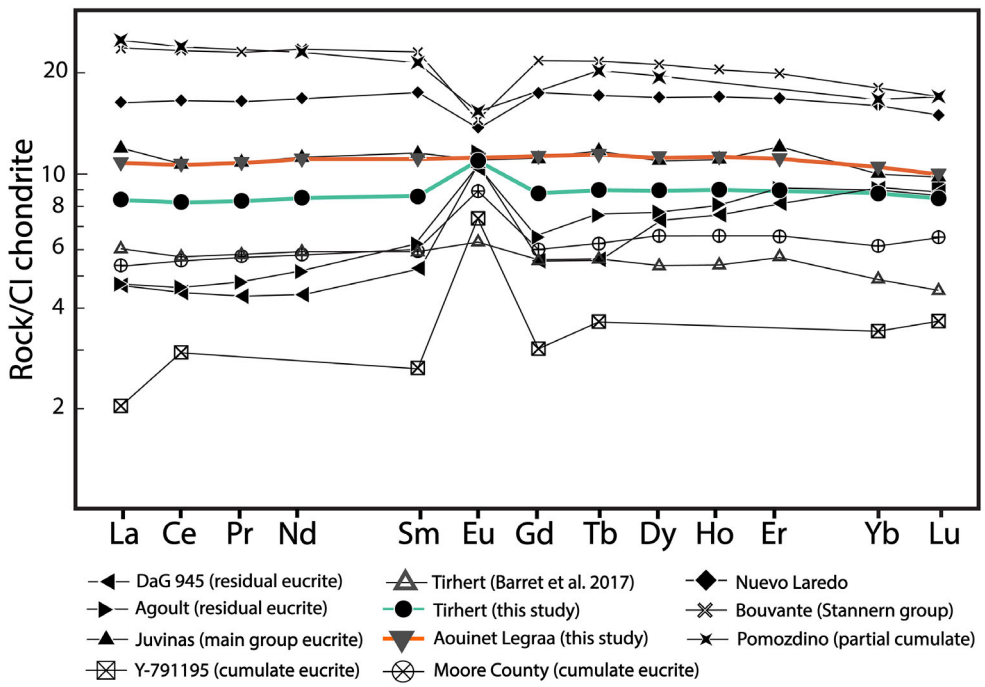

Fig. 8. REE patterns of Tirhert and Aouinet Legraa compared to the REE patterns of main group, Stannern, Nuevo Laredo, residual, partial cumulate and cumulate eucrites. Data are from Mittlefehldt & Lindstrom (1993), Barrat et al. (2007), Warren et al. (1990, 2009), Yamaguchi et al. (2009) and Barret et al. (2017). REE composition of Tirhert reported in the work of Barret et al. (2017). (Color figure can be viewed at wileyonlinelibrary.com.)

that cut through the exsolved lamellae (Fig. S3c). Plagioclase contains widespread inclusions (10 μm diameter) of high-Ca pyroxene, phosphates, and troilite, and clouding is often dense along twin boundaries. Late-stage mesostasis is abundant and mostly occurs between plagioclase laths (Fig. 10a; Fig. S5 in supporting information). The silica phase in Aouinet Legraa occurs mostly in granular mesostasis, associated with high-Ca pyroxene, subhedral to euhedral ilmenite, some troilite, phosphates, and zircon. The remaining silica is intergrown with plagioclase and often contains pyroxene, plagioclase, and troilite inclusions. Oxides occur as scattered subhedral to anhedral grains up to 70 μm in size in contact with pyroxene and plagioclase or as micrometer-sized grains in mesostasis (Fig. 10a; Fig. S5). Fe-metal was also detected in a single area of Aouinet Legraa in association with plagioclase, zircon, and chromite with exsolved ilmenite (Fig. 10b).

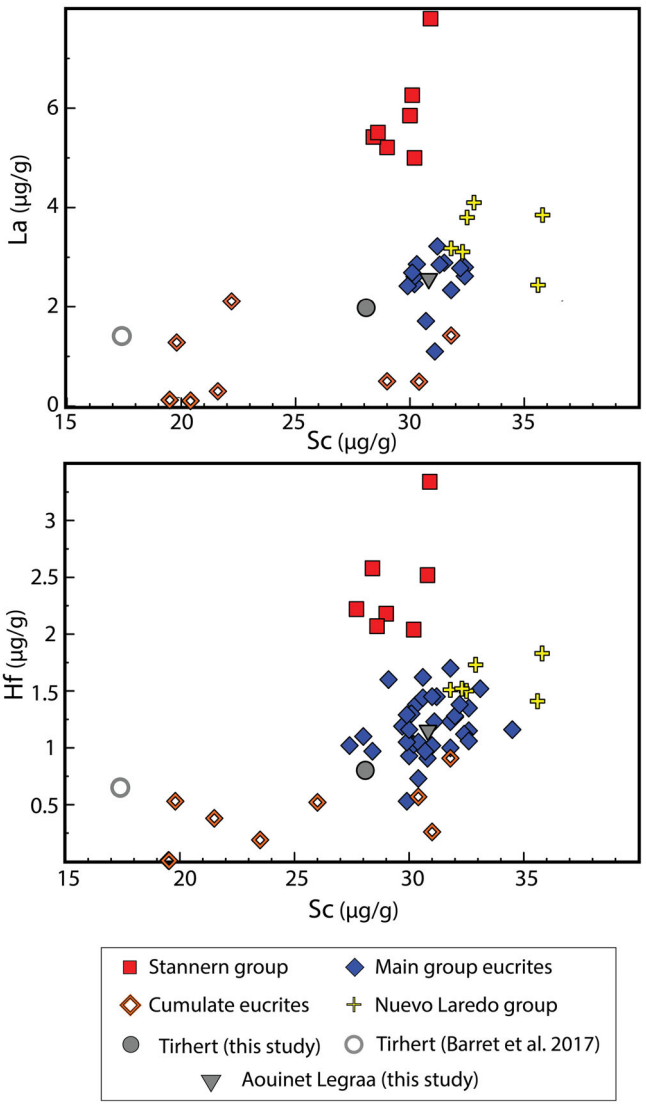

Fig. 9. Sc (µg/g) versus La (µg/g) and Hf (µg/g) compositions in Tirhert and Aouinet Legraa, plotted with values measured in cumulate eucrites, main group, Nuevo Laredo and Stannern eucrites. Values measured in Tirhert and reported in Barret et al. (2017) are also plotted. (Color figure can be viewed at wileyonlinelibrary.com.)

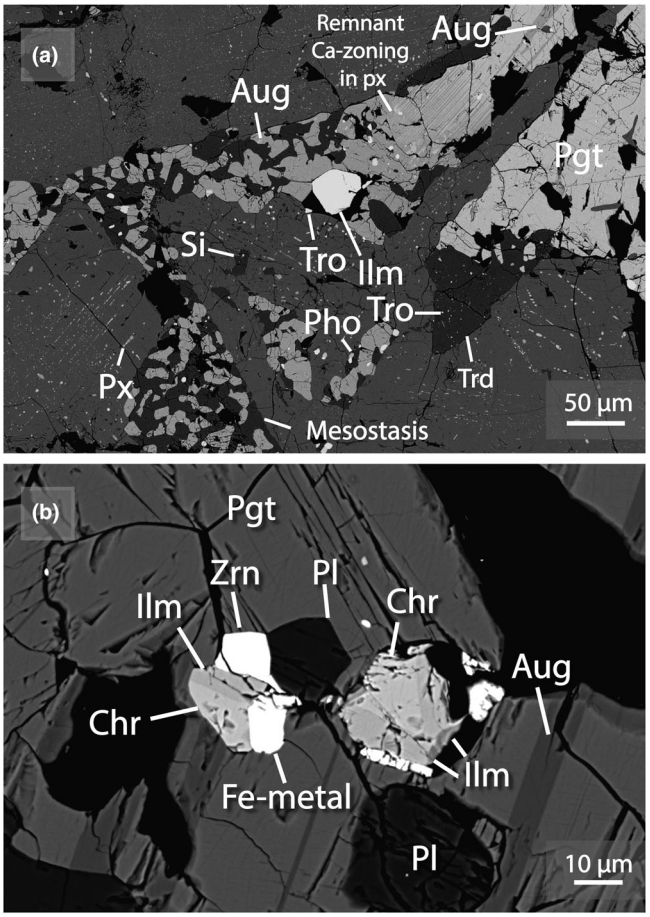

Fig. 10. BSE images of Aouinet Legraa. a) Plagioclase laths enclosed by pyroxene in Aouinet Legraa. The main mineral phase is pigeonite containing exsolution lamellae of augite. Clouding is extremely dense in plagioclase. Mesostasis domains have a granular texture. Note the occurrence of remnant Ca-zoning in pyroxene adjacent to mesostasis. b) Chromite with exsolution lamellae of ilmenite, in close contact with zircon, Fe-metal. Px = pyroxene; Pgt = pigeonite; Aug = augite; Pl = plagioclase; Trd = tridymite; Chr = chromite; Ilm = ilmenite; Tro = troilite; Pho = phosphates; Zrn = zircon.

Mineral Compositions

The endmember compositions of pyroxene in Aouinet Legraa follow the Fe-Ca trend (Fig. 5b; Table 1). The average Fe/Mn ratios is ~33, which is consistent with values from basaltic eucrites (Fig. S7). The average composition of low-Ca pyroxene is $En_{35\pm0.34}Fs_{59\pm0.65}Wo_{6\pm0.43}$ (n = 7; Mg# = 37). Exsolved augite is $En_{29\pm0.4}Fs_{30\pm0.3}Wo_{41\pm0.5}$ (n = 12) on average. The composition of the rim in the pyroxenes with remnant Ca-zoning is $En_{30}Fs_{28}Wo_{42}$, changing to $En_{35}Fs_{58}Wo_{7}$ in the core. The minor elements in pyroxene are extensively homogenized, with little variation of the Al and Ti contents (Fig. 5b).

Plagioclase in Aouinet Legraa is slightly zoned, with endmember compositions ranging from An_{82} to An_{89} (Fig. 6b; Table 2). The compositions of plagioclase inclusions in pyroxene are similar to those of igneous plagioclase (Table 2). The K (afu) and An (%) of plagioclase fall within the range of HED meteorites (Fig. S8).

The minor phases in Aouinet Legraa are silica, chromite, ulvöspinel, ilmenite, troilite, phosphates, zircon, and Fe-metal. The EPMA data of oxides and silica in Aouinet Legraa are given in Tables 3 and 4, respectively. The compositions of chromite and ulvöspinel are plotted in Fig. 7. Raman spectroscopy

data showed that the silica phase in Aouinet Legraa is monoclinic tridymite (see Fig. S9). The dominant spinel phase in Aouinet Legraa is ulvöspinel (up to $Usp_{56}Chr_{41}$). Chromite (Fig. 10b) in Aouinet Legraa is $Chr_{58}Usp_{24}Spl_{16}$ and contains exsolution lamellae of ilmenite with ~0.5 wt% Cr_2O_3, 0.9 wt% MgO, and 0.8 wt% MnO. Adjacent plagioclase grains are $An_{87.7}Ab_{11.7}Or_{0.6}$ and $An_{89.5}Ab_{10}Or_{0.4}$. Fe-metal is also detected in association with subhedral zircon up to ~10 μm in size with ZrO_2 and TiO_2 contents of 64 and 0.2 wt%, respectively (Table S4 in supporting information). Ilmenite contains 52 wt% TiO_2 and ~45 wt% FeO, which is in the range of ilmenite compositions in basaltic eucrites (Mayne et al., 2009; Mittlefehldt, 2015).

Trace and Rare Element Composition

The bulk composition of Aouinet Legraa is listed in Table 5, and its REE pattern is plotted in Fig. 8 with other eucritic geochemical groups. This rock has a flat REE pattern with no Eu anomaly (i.e., Eu/Eu* = ~1), and REE abundances of about ~10 × CI. The abundances of Sc, La, and Hf in this rock fall in the range of the main group eucrite values (Fig. 9).

DISCUSSION

Classification

The composition of host pyroxenes in Tirhert and Aouinet Legraa overlaps with that of basaltic eucrites (Fig. 5; En_{45-33}; Mayne et al., 2009; Mittlefehldt et al., 1998). Pyroxenes in Aouinet Legraa are more ferroan than those in Tirhert, and contain augite lamellae with a higher CaO content (wt%). Plagioclase compositions in both meteorites range from An_{82} to An_{91}, which is identical to compositional ranges of basaltic eucrites (Fig. 6; An_{74-92}; Mayne et al., 2009; Mittlefehldt, 2015; Warren & Jerde, 1987).

The bulk composition of Tirhert and Aouinet Legraa is further evidence that these meteorites were collected shortly after their fall to the Earth's surface and belong to the HED suite. Previous studies have shown that hot and cold desert weathering can affect the bulk elemental concentration of meteorites (Barrat et al., 1999, 2003; Crozaz et al., 2003; Folco et al., 2000). Barrat et al. (2003) reported that the concentration of REEs is not significantly affected in the finds from the Sahara. However, these meteorites show a striking increase in Ba, Sr, and Pb abundances, due to the formation of secondary products (calcite and gypsum) and terrestrial contamination by Pb. Antarctic finds generally have much higher Hf/Sm values than unweathered meteorites or finds from the Sahara (Crozaz et al., 2003). These ratios can range from 0.5 to 3.2 for Antarctic finds (Mittlefehldt & Lindstrom, 1991), but are generally chondritic for unweathered eucrites (Hf/Sm = 0.72 ± 0.04; Barrat et al., 2000, 2003). Ba and Sr concentrations in Tirhert and Aouinet Legraa are within the range of those measured in eucrite falls (Barrat et al., 2003). The ratios of Hf/Sm and Th/U in Tirhert are chondritic and are 0.63 and 4, respectively. Comparable ratios are also observed in Aouinet Legraa (Hf/Sm = 0.7; Th/U = 4). Note that this rock has a very low Pb content (58 ng g^{-1}) compared to most basaltic eucrites.

The trace element abundances in Aouinet Legraa are very similar to those of Juvinas, as evidenced by its flat REE pattern, its REE abundances of about 10 × CI, and its concentrations of the elements Sc, Hf, V, and Ba (Figs. 8 and 9; Table 5). This confirms its grouping with main group eucrites.

We showed in Figs. 8 and 9 that the trace element abundances in Tirhert differ from those of main group eucrites like Aouinet Legraa and Juvinas, and also from the abundances of cumulate eucrites like Moore County, the most incompatible element-rich cumulate eucrite (Mittlefehldt & Lindstrom, 1993). In what follows, we explore some of the similarities and the differences between Tirhert and other basaltic and cumulate eucrites in order to constrain its possible origin: (1) Tirhert has an REE pattern of about eight to nine times CI, and falls between the REE patterns of Moore County (5–7 × CI) and Juvinas (~10 × CI). Similarly, in a plot of Sc versus La and Hf, Tirhert falls between the field of main group and cumulate eucrites (Fig. 9). (2) The positive Eu anomaly displayed by Tirhert indicates plagioclase accumulation. This is similar to the characteristics of cumulate eucrites like Moore County (Fig. 8). (3) Tirhert has pyroxenes with lower Mg# (up to 43), unlike Moore County (Mg# = 55; Mittlefehldt & Lindstrom, 1993). (4) The modal abundance of plagioclase in Tirhert is up to ~50% in the section studied, up to 6% higher than Moore County (Mayne et al., 2009), but very similar to the rare feldspar cumulate Medanitos (48% plagioclase; Delaney et al., 1983). In short, Tirhert is coarse-grained and has seemingly accumulated plagioclase, its pyroxene has lower Mg# than Moore County, and it has an intermediate trace element abundance between main group eucrites and cumulate eucrites. These features suggest that Tirhert might be a partial cumulate from a main group magma, or a flotation cumulate formed in a subvolcanic chamber, or by scavenging crystals during eruption. Decoupling of Mg# of pyroxene and the REE concentrations is identified in a very restricted number of eucrites. For example, the partial cumulate Pomozdino contains pyroxene with Mg# of ~47, but

has a higher abundance of REEs similar to that displayed by Stannern eucrites (Fig. 8) (Warren et al., 1990). Y-791195 is a cumulate eucrite containing pyroxene with Mg# of 45, very close to that measured in Tirhert's most magnesian pyroxene (Mg# = 43); however, this eucrite has REE abundances lower than those in Moore County (Fig. 8). Mittlefehldt and Lindstrom (1993) suggested that Y-791195 formed from a more evolved melt than Moore County, but contains less trapped intercumulus material compared to it. This could suggest that Tirhert formed from a slightly more ferroan and evolved melt than Y-791195, and contains an important amount of trapped melt, higher than Moore County.

Another possible explanation of this decoupling could include sample heterogeneity during bulk analysis, due to the coarse-grained nature of Tirhert. The trace element abundances of Tirhert from Barrett et al. (2017) differ from the ones presented in this work (Figs. 8 and 9). Their results show that Tirhert has a nearly flat REE pattern with no significant positive Eu anomaly, and it is about $\sim 6 \times$ CI. This mainly could be due to the low mass they used for their bulk analysis (0.11330 g). Phosphates are the main carriers of REEs in eucrites (Hsu & Crozaz, 1996). Thus, the undersampling or the heterogeneous distribution of these phases in the sample would lead to an REE-depleted (mainly light REE [LREE]) pattern and a positive Eu anomaly (Yamaguchi et al., 2009). In this work, the REE pattern of Tirhert is significantly flat and not depleted in LREEs, and the positive Eu anomaly is most likely due to accumulation of plagioclase.

Could the composition of Tirhert be the result of partial melting of main group eucrites? Residual eucrites display an REE-depleted pattern with positive Eu anomalies like cumulate eucrites (Fig. 8) (Yamaguchi et al., 2009). However, as shown by these authors, the main characteristic of this group of noncumulate eucrites is their low LREE abundances. This is not observed in Tirhert, ruling out a residual origin for this eucrite.

Textural and Compositional Evidence for Post-Crystallization Metamorphism

Numerous studies reported that most eucrites underwent thermal metamorphism (Glass & Simonson, 2012; Harlow & Klimentidis, 1980; Iizuka et al., 2015; Metzler et al., 1995; Takeda & Graham, 1991; Yamaguchi et al., 1996, 1997, 2009). This is reflected in a pronounced modification of their original igneous textures and a chemical equilibration of the minerals that compose them. Yamaguchi et al. (1996, 1997) suggested rapid eruptions and subsequent burial of the basalts, supported by internal heat as thermal sources. Therefore, the oldest eucrites, and consequently the most metamorphosed (type 4–7 eucrites; Takeda & Graham, 1991; Yamaguchi et al., 1996), are buried deep in the crust, while the youngest and least metamorphosed are at the surface (type 1–3 eucrites; Takeda & Graham, 1991). Equilibration temperatures were estimated from pyroxene thermometry to be 650–1100 °C, which is slightly higher than the crystallization temperature of eucritic material (1060 °C; Stolper, 1977).

Tirhert and Aouinet Legraa exhibit a number of textural and compositional features that indicate they were exposed to significantly different post-crystallization temperatures, and had distinct slow cooling histories. The most important features are as follows. (1) Aouinet Legraa appears to have retained its original igneous texture (subophitic). Tirhert was most likely exposed to a higher metamorphic temperature that partly modified its texture. The presence of plagioclase laths with curved margins indicates a subophitic texture that was altered by metamorphism (Fig. S3b). (2) Tirhert, unlike Aouinet Legraa, is devoid of mesostasis domains (except the area shown in Fig. S3b). It has been shown by Barrat et al. (2007) that the most metamorphosed, partially melted eucrites lack mesostasis. This could explain the presence of such late phases in Aouinet Legraa, but not in Tirhert. (3) Pyroxene and plagioclase in Tirhert are rarely clouded compared to Aouinet Legraa. This suggests complete exsolution of inclusions in the major mineral phases during annealing. (4) Pyroxene in both meteorites is homogenized except for some areas where the initial igneous Ca-zoning is still preserved. We showed that the pyroxene with remnant Ca-zoning is more common in Aouinet Legraa than Tirhert. This could be due to differences in peak temperatures during metamorphism. It has been shown that rapidly cooled eucrites contain zoned pyroxenes with Mg-rich cores and Fe- and Ca-rich rims (the Mg-Fe-Ca trend; Takeda & Graham, 1991; Yamaguchi et al., 1996). Yamaguchi et al. (1996) reported that, in order to completely erase the Ca zoning of primary pigeonite, the peak metamorphic temperatures should exceed the pyroxene solvus ($\sim$1000 °C); this implies that homogenization of Fe and Mg can occur while the igneous Ca-zoning is preserved. Based on this, in the case of Tirhert, it is most likely that the peak metamorphic temperature was not maintained for a long enough period of time at or above the pyroxene solvus to completely erase the Ca zoning of all primary pyroxenes, which explains why some of them still preserve it. This metamorphic event led to the homogenization of the major elements in pyroxene (except Ca in some cases), and the partial

homogenization of the minor elements in pyroxene, as well as plagioclase. In the case of Aouinet Legraa, remnant Ca-zoning in pyroxene is abundant. This suggests that this rock has been subjected to peak metamorphic temperatures at or slightly above the pyroxene solvus (~1000 °C) for a shorter period of time than Tirhert. This led to the preservation of Ca-zoning in the majority of pyroxenes while homogenizing their Fe and Mg contents, as well as the homogenization of minor elements in pyroxenes, and the preservation, to some extent, of the initial zoning in plagioclase. These findings are further evidence that Aouinet Legraa is less metamorphosed than Tirhert. (5) Exsolution lamellae of ilmenite in chromite have been previously identified in Apollo and eucritic samples (El Goresy et al., 1972; Gardner-Vandy et al., 2011; Steele & Smith, 1976) and have been attributed to subsolidus reduction of Cr-spinel during a metamorphic event. This scenario is best suited to explain the exsolution of ilmenite from chromite in Tirhert and Aouinet Legraa. This is also supported by the presence of Fe-metal and troilite in close proximity to the exsolved chromite grains (Figs. 4b and 10b). Our results suggest that Tirhert is more metamorphosed than Aouinet Legraa. We conclude that both meteorites belong to type 4–5 eucrites, as indicated by the degree of equilibration of their major mineral phases, the occurrence of remnant Ca-zoning in pyroxene, and the absence of inverted pigeonite.

Spinel compositions have proved useful in constraining the metamorphic histories of eucrites. Metamorphosed eucrites (types 4–5) tend to have more Ti-enriched spinels compared to unequilibrated eucrites (types 1–2; Yamaguchi, 2000). The compositions of chromite and ulvöspinel in Tirhert and Aouinet Legraa are in the range of types 5–6 eucrites. This is consistent with the general features of texture and composition presented above.

Temperature of Equilibration

To calculate the equilibration temperatures, we used the QUILF program (Andersen et al., 1993). The QUILF input data can be found in Table S5. The temperatures derived from pigeonite and augite pairs in Tirhert and Aouinet Legraa are 931 ± 53 °C and 758 ± 10 °C, respectively. These temperatures are within the range of equilibrated eucrites (650–1100 °C; Mayne et al., 2009) and support our conclusion that Tirhert underwent prolonged thermal metamorphism and slow cooling in depth.

Examination for Evidence of Metasomatism

In addition to metamorphism, a number of eucrites have been found to contain secondary alteration features commonly indicated by the occurrence of quartz veinlets (Treiman et al., 2004), fayalitic olivine veinlets filling fractures in pyroxene (Barrat et al., 2011; Mayne et al., 2016; Pang et al., 2017; Patzer & McSween, 2018; Roszjar et al., 2011; Vollmer et al., 2020; Warren et al., 2014), and the breakdown of pyroxene to silica and troilite (Chen et al., 2015; Mayne et al., 2016; Zhang et al., 2013). According to Barrat et al. (2011), the deposit of fayalitic veinlets is attributed to Fe-metasomatism, which progressively affected eucritic pyroxenes following a three-stage scheme: (1) Fe-enrichment along fractures in pyroxene, (2) fayalitic and anorthitic veinlets filling fractures in pyroxene, (3) Al-depletion in pyroxene. These features have been mostly found confined to unequilibrated pyroxenes; however, in some cases, they also occur in equilibrated pyroxenes (Barrat et al., 2011, Pang et al., 2017; Shisseh et al., 2020). In this study, we examined the large-scale SEM mosaics, EDS maps, and EPMA data in order to assess whether Tirhert and Aouinet Legraa were affected by metasomatism, and found no evidence of it. However, we cannot rule out the possibility that some of these metasomatic features (e.g., Fe-enrichment in pyroxene, if occurred) were erased during the metamorphic event that led to the equilibration of these rocks.

Shock Effects

Tirhert contains fractured plagioclase and pyroxene. Inclusions in these minerals are also affected, suggesting that metamorphism occurred before the shock (Fig. 4a; Fig. S4). These features are consistent with the shock degree A (very weakly shocked eucrites) based on Kanemaru et al. (2020). Aouinet Legraa experienced a higher degree of shock (shock degree B or C; Kanemaru et al., 2020). This is evidenced by the occurrence of pervasive fracturing in the major mineral phases and mosaicism in pyroxene (Fig. 10a; Fig. S3c). Clouding in shocked plagioclase is often chaotic (Fig. S5). Inclusions do not follow crystallographic directions and are usually scattered in close proximity to large fractures. Cracks in pyroxene are often filled with plagioclase and chromite blebs and lenses (Fig. 10a; Fig. S5). These cracks probably served as nuclei that allowed the crystallization of these phases.

SUMMARY AND CONCLUSIONS

Tirhert and Aouinet Legraa are rare unbrecciated eucrite falls. Both samples are covered by a fusion crust typical of eucrites and an interior dominated by plagioclase, pyroxene, and minor opaque components. Based on our petrographic and geochemical investigation, we conclude the following:

1. Aouinet Legraa has a subophitic texture typical of rapidly cooled basaltic eucrites. Tirhert is poikilitic with remnant subophitic pockets. Pyroxene in both meteorites is mainly pigeonite with exsolution lamellae of augite. Pigeonite in Aouinet Legraa is more ferroan than that of Tirhert. Plagioclase in Aouinet Legraa retained some of its initial igneous zoning, and it is less calcic.
2. The trace element abundances of both meteorites suggest that they have distinct origins. Aouinet Legraa belongs to main group eucrites, whereas Tirhert, in case of sample homogeneity during meteorite bulk analysis, could be a partial cumulate or flotation cumulate formed by flotation of plagioclase in a subvolcanic chamber, or by scavenging crystals during eruption.
3. Tirhert and Aouinet Legraa have undergone thermal metamorphism and slow cooling as indicated by the equilibration of major mineral phases, clouding, and spinel composition. Textural and compositional studies led us to conclude that Tirhert is more metamorphosed than Aouinet Legraa. This was supported by the equilibration temperatures obtained by the QUILF program using pigeonite and augite pairs in Tirhert (~930 °C) and Aouinet Legraa (~758 °C).
4. Taking into account that the degree of metamorphism correlates with burial depth, we conclude that Tirhert, in contrast to Aouinet Legraa, was most likely ejected from a deeper region of the Vestan crust.

Acknowledgments—We greatly appreciate the reviews and the constructive comments of Dr. Allan Treiman and an anonymous reviewer. We also thank Dr. Michael Zolensky for editorial handling. The analyses were funded by the Erasmus+ program (National Museum of Natural History of Paris, France and the University of Pisa, Italy) and the Fulbright Joint-Supervision program (institute of Meteoritics, University of New Mexico, USA). We kindly thank Daryl Pitt for providing a sample of Aouinet Legraa. We thank Roger Hewins, Brigitte Zanda, Emmanuel Jacquet, and Sylvain Pont for their valuable advice and support during this work. We thank Pr. Luigi Folco for his advice regarding the QUILF program. Oulfa Belhadj is thanked for her help during the Raman spectroscopy session. We also thank Nicolas Rividi and Michel Fialin (Service Camparis, Sorbonne Université, Paris, France) for their technical assistance during the EPMA sessions. We appreciate the helpful advice of David W. Mittlefehldt and Jean-Alix Barrat, which greatly improved this work. This study is part of the ATTARIK Foundation for Meteoritics and Planetary Science, which is dedicated to the promotion of these sciences in Morocco, Arab countries, and Africa www.attarikfoundation.org.

Data Availability Statement—The data that support the findings of this study are available in the supplementary material of this article.

Editorial Handling—Dr. Michael Zolensky

REFERENCES

Andersen, D. J., Lindsley, D. H., and Davidson, P. M. 1993. QUILF: A Pascal Program to Assess Equilibria Among Fe-Mg-Mn-Ti Oxides, Pyroxenes, Olivine, and Quartz. *Computers & Geosciences* 19: 1333–50.

Barrat, J. A., Blichert-Toft, J., Gillet, P., and Keller, F. 2000. The Differentiation of Eucrites: The Role of In Situ Crystallization. *Meteoritics & Planetary Science* 35: 1087–100.

Barrat, J. A., Dauphas, N., Gillet, P., Bollinger, C., Etoubleau, J., Bischoff, A., and Yamaguchi, A. 2016. Evidence from Tm Anomalies for Non-CI Refractory Lithophile Element Proportions in Terrestrial Planets and Achondrites. *Geochimica et Cosmochimica Acta* 176: 1–17.

Barrat, J. A., Gillet, P., Lesourd, M., Blichert-Toft, J., and Poupeau, G. R. 1999. The Tatahouine Diogenite: Mineralogical and Chemical Effects of Sixty-Three Years of Terrestrial Residence. *Meteoritics & Planetary Science* 34: 91–7.

Barrat, J. A., Jambon, A., Bohn, M., Blichert-Toft, J., Sautter, V., Göpel, C., Gillet, P., Boudouma, O., and Keller, F. 2003. Petrology and Geochemistry of the Unbrecciated Achondrite Northwest Africa 1240 (NWA 1240): An HED Parent Body Impact Melt. *Geochimica et Cosmochimica Acta* 67: 3959–70.

Barrat, J. A., Yamaguchi, A., Bunch, T. E., Bohn, M., Bollinger, C., and Ceuleneer, G. 2011. Possible Fluid-Rock Interactions on Differentiated Asteroids Recorded in Eucritic Meteorites. *Geochimica et Cosmochimica Acta* 75: 3839–52.

Barrat, J. A., Yamaguchi, A., Greenwood, R. C., Bohn, M., Cotten, J., Benoit, M., and Franchi, I. A. 2007. The Stannern Trend Eucrites: Contamination of Main Group Eucritic Magmas by Crustal Partial Melts. *Geochimica et Cosmochimica Acta* 71: 4108–24.

Barrat, J. A., Zanda, B., Moynier, F., Bollinger, C., Liozou, C., and Bayon, G. 2012. Geochemistry of CI Chondrites: Major and Trace Elements, and CU and Zn Isotopes. *Geochimica et Cosmochimica Acta* 83: 79–92.

Barrett, T. J., Mittlefehldt, D. W., Greenwood, R. C., Charlier, B. L. A., Hammond, S. J., Ross, D. K., and Grady, M. M. 2017. The Mineralogy, Petrology, and Composition of Anomalous Eucrite Emmaville. *Meteoritics & Planetary Science* 52: 656–68.

Binzel, R. P., and Xu, S. 1993. Chips off Asteroid 4 Vesta: Evidence for the Parent Body of Basaltic Achondrite Meteorites. *Science* 260: 186–91.

Bouvier, A., Gattacceca, J., Grossman, J., and Metzler, K. 2017. The Meteoritical Bulletin, No. 105. *Meteoritics & Planetary Science* 52: 2411–1.

Burbine, T. H., Buchanan, P. C., Binzel, R. P., Bus, S. J., Hiroi, T., Hinrichs, J. L., Meibom, A., and McCoy, T. J. 2001. Vesta, Vestoids, and the Howardite, Eucrite, Diogenite Group: Relationships and the Origin of Spectral Differences. *Meteoritics & Planetary Science* 36: 761–81.

Chen H. Y., Miao B. K., and Huang L. L. 2015. Ancient Silicification on Asteroid 4 Vesta: Evidence from a Eucrite Grove Mountains (GRV) 13001 from Antarctic (Abstract #5003). 78th Meeting of the Meteoritical Society.

Chennaoui Aoudjehane, H., Agee, C. B., Aaranson, A., and Bouragaa, A. 2016. Sidi Ali Ou Azza (L4): A New Moroccan Fall (Abstract #6120). 79th Meeting of the Meteoritical Society.

Chennaoui Aoudjehane, H., Avice, G., Barrat, J. A., Boudouma, O., Chen, G., Duke, M. J. M., Franchi, I. A., et al. 2012. Tissint Martian Meteorite: A Fresh Look at the Interior, Surface, and Atmosphere of Mars. *Science* 338: 785–8.

Chennaoui Aoudjehane, H., and Garvie, L.A.J. 2018. Kheneg Ljouâd (Morocco): The Unique LL5/6 Meteorite Fall (Abstract #6050). 81st Annual Meeting of the Meteoritical Society.

Connelly, J. N., Bollard, J., and Bizzarro, M. 2017. Pb–Pb Chronometry and the Early Solar System. *Geochimica et Cosmochimica Acta* 201: 345–63.

Consolmagno, G. J., Golabek, G. J., Turrini, D., Jutzi, M., Sirono, S. I., Svetsov, V., and Tsiganis, K. 2015. Is Vesta an Intact and Pristine Protoplanet? *Icarus* 254: 190–201.

Crozaz, G., Floss, C., and Wadhwa, M. 2003. Chemical Alteration and REE Mobilization in Meteorites from Hot and Cold Deserts. *Geochimica et Cosmochimica Acta* 67: 4727–41.

De Sanctis, M. C., Ammannito, E., Capria, M. T., Capaccioni, F., Combe, J.-P., Frigeri, A., Longobardo, A., et al. 2013. Vesta's Mineralogical Composition as Revealed by the Visible and Infrared Spectrometer on Dawn. *Meteoritics & Planetary Science* 48: 2166–84.

Delaney, J. S., Nehru, C. E., and Prinz, M. (1983) The Medanitos Feldspar Cumulate Eucrite (Abstract). 14th Lunar and Planetary Science Conference. pp. 150–151.

El Goresy, A., Taylor, L. A., and Ramdohr, P. 1972. Fra Mauro Crystalline Rocks: Mineralogy, Geochemistry, and Subsolidus Reduction of the Opaque Minerals. Proceedings, 3rd Lunar and Planetary Science Conference. pp. 333–49.

Folco, L., Franchi, I. A., D'orazio, M., Rocchi, S., and Schultz, L. 2000. A New Martian Meteorite from the Sahara: The Shergottite Dar al Gani 489. *Meteoritics & Planetary Science* 35: 827–39.

Gardner-Vandy, K. G., Hill, D. H., Lauretta, D. S., Goreva, Y. S., Domanik, K. J., Greenwood, R. C., and Killgore, M. 2011. Petrology and Geochemistry of the Northwest Africa 3368 Eucrite. *Meteoritics & Planetary Science* 46: 1052–70.

Glass, B. P., and Simonson, B. M. 2012. Distal Impact Ejecta Layers: Spherules and More. *Elements* 8: 43–8.

Harlow, G. E., and Klimentidis, R. 1980. Clouding of Pyroxene and Plagioclase in Eucrites—Implications for Post-Crystallization Processing. 11th Lunar and Planetary Science Conference. pp. 1131–1143.

Hsu, W., and Crozaz, G. 1996. Mineral Chemistry and the Petrogenesis of Eucrites: I Non-Cumulate Eucrites. *Geochimica et Cosmochimica Acta* 60: 4571–91.

Iizuka, T., Yamaguchi, A., Haba, M. K., Amelin, Y., Holden, P., Zink, S., and Ireland, T. R. 2015. Timing of Global Crustal Metamorphism on Vesta as Revealed by High-Precision U–Pb Dating and Trace Element Chemistry of Eucrite Zircon. *Earth and Planetary Science Letters* 409: 182–92.

Kanemaru, R., Imae, N., Yamaguchi, A., Takenouchi, A., and Nishido, H. 2020. Estimation of Shock Degrees of Eucrites Using X-ray Diffraction and Petrographic Methods. *Polar Science* 26: 100605.

Kleine, T., Touboul, M., Bourdon, B., Nimmo, F., Mezger, K., Palme, H., Stein, B. J., Qing-Zhu, Y., and Halliday, A. N. 2009. Hf–W Chronology of the Accretion and Early Evolution of Asteroids and Terrestrial Planets. *Geochimica et Cosmochimica Acta* 73: 5150–88.

Kleine, K., and Wadhwa, M. 2017. Chronology of Planetesimal Differentiation. In *Planetesimals: Early Differentiation and Consequences*, edited by L. T. Elkins-Tanton and B. P. Weiss, 224–45. Cambridge: Cambridge University Press.

Lorenz, K. A., Nazarov, M. A., Kurat, G., Brandstaetter, F., and Ntaflos, T. 2007. Foreign Meteoritic Material of Howardites and Polymict Eucrites. *Petrology* 15: 109–25.

Marchi, S., McSween, H. Y., O'Brien, D. P., Schenk, P., De Sanctis, M. C., Gaskell, R., Jaumann, R., et al. 2012. The Violent Collisional History of Asteroid 4 Vesta. *Science* 336: 690–4.

Mayne, R. G., McSween, H. Y., Jr., McCoy, T. J., and Gale, A. 2009. Petrology of the Unbrecciated Eucrites. *Geochimica et Cosmochimica Acta* 73: 794–819.

Mayne, R. G., Smith, S. E., and Corrigan, C. M. 2016. Hiding in the Howardites: Unequilibrated Eucrite Clasts as a Guide to the Formation of Vesta's Crust. *Meteoritics & Planetary Science* 51: 2387–402.

McCoy, T. J., Beck, A. W., Prettyman, T. H., and Mittlefehldt, D. W. 2015. Asteroid (4) Vesta II: Exploring a Geologically and Geochemically Complex World with the Dawn Mission. *Geochemistry* 75: 273–85.

McSween, H. Y., Binzel, R. P., De Sanctis, M. C., Ammannito, E., Prettyman, T. H., Beck, A. W., Reddy, V., et al. 2013. Dawn: The Vesta-HED Connection; and the Geologic Context for Eucrites, Diogenites, and Howardites. *Meteoritics & Planetary Science* 48: 2090–104.

Metzler, K., Bobe, K. D., Palme, H., Spettel, B., and Stöffler, D. 1995. Thermal and Impact Metamorphism on the HED Parent Asteroid. *Planetary and Space Science* 43: 499–525.

Mittlefehldt, D. W. 2015. Asteroid (4) Vesta: I. The Howardite-Eucrite-Diogenite (HED) Clan of Meteorites. *Chemie der Erde-Geochemistry* 75: 155–83.

Mittlefehldt, D. W., and Lindstrom, M. M. 1991. Generation of Abnormal Trace Element Abundances in Antarctic Eucrites by Weathering Processes. *Geochimica et Cosmochimica Acta* 55: 77–87.

Mittlefehldt, D. W., and Lindstrom, M. M. 1993. Geochemistry and Petrology of a Suite of Ten Yamato HED Meteorites. *Proceedings of the NIPR Symposium on Antarctic Meteorites* 6: 268–92.

Mittlefehldt, D. W., McCoy, T. J., Goodrich, C. A., and Kracher, A. 1998. Non-Chondritic Meteorites from Asteroidal Bodies. In *Planetary Materials*, edited by J. J. Papike, 4-1–4-195. Washington, DC: Mineralogical Society of America.

Neumann, W., Breuer, D., and Spohn, T. 2014. Differentiation of Vesta: Implications for a Shallow Magma Ocean. *Earth and Planetary Science Letters* 395: 267–80.

Pang, R. L., Zhang, A. C., and Wang, R. C. 2017. Complex Origins of Silicate Veinlets in HED Meteorites: A Case Study of Northwest Africa 1109. *Meteoritics & Planetary Science* 52: 2113–31.

Papike J. J. 1998. Comparative Planetary Mineralogy: Chemistry of Melt-Derived Pyroxene, Feldspar and Olivine. In *Planetary materials*, edited by Papike J. J., *Reviews in Mineralogy*, vol. 36. Washington, DC: Mineralogical Society of America. pp. 7-1–7-11.

Patzer, A., and McSween, H. Y. 2018. Ferroan Olivine-Bearing Eucrite Clasts Found in Howardites. *Meteoritics & Planetary Science* 53: 1131–49.

Roszjar, J., Metzler, K., Bischoff, A., Barrat, J. A., Geisler, T., Greenwood, R. C., Franchi, I. A., and Klemme, S. 2011. Thermal History of Northwest Africa 5073: A Coarse-Grained Stannern-Trend Eucrite Containing cm-Sized Pyroxenes and Large Zircon Grains. *Meteoritics & Planetary Science* 46: 1754–73.

Roszjar, J., Whitehouse, M. J., Srinivasan, G., Mezger, K., Scherer, E. E., Van Orman, J. A., and Bischoff, A. 2016. Prolonged Magmatism on 4 Vesta Inferred from Hf-W Analysis of Eucrite Zircon. *Earth and Planetary Science Letters* 452: 216–26.

Russell, C. T., Raymond, C. A., Coradini, A., McSween, H. Y., Zuber, M. T., Nathues, A., De Sanctis, M. C., et al. 2012. Dawn at Vesta: Testing the Protoplanetary Paradigm. *Science* 336: 684–6.

Ruzicka, A., Grossman, J., Bouvier, A., and Agee, C. B. 2017. The Meteoritical Bulletin No. 103. *Meteoritics & Planetary Science* 52: 1014.

Schiller, M., Baker, J., Creech, J., Paton, C., Millet, M. A., Irving, A., and Bizzarro, M. 2011. Rapid Timescales for Magma Ocean Crystallization on the Howardite-Eucrite-Diogenite Parent Body. *The Astrophysical Journal Letters* 740: L22.

Schwartz, J. M., and McCallum, I. S. 2005. Comparative Study of Equilibrated and Unequilibrated Eucrites: Subsolidus Thermal Histories of Haraiya and Pasamonte. *American Mineralogist* 90: 1871–86.

Shisseh T., Chennaoui Aoudjehane H., Zanda B., Hewins R., Pont S., Folco L., Agee C. B., and Jacquet E. 2020. Northwest Africa 11911: Polymict Rock from Vesta with a Variety of Secondary Alteration Features (Abstract #2658). 51st Lunar and Planetary Science Conference. CD-ROM.

Steele, I. M., and Smith, J. V. 1976. Mineralogy of the Ibitira Eucrite and Comparison with Other Eucrites and Lunar Samples. *Earth and Planetary Science Letters* 33: 67–78.

Stolper, E. 1977. Experimental Petrology of Eucritic Meteorites. *Geochimica et Cosmochimica Acta* 41: 587–611.

Takeda, H., and Graham, A. L. 1991. Degree of Equilibration of Eucritic Pyroxenes and Thermal Metamorphism of the Earliest Planetary Crust. *Meteoritics* 26: 129–34.

Touboul, M., Sprung, P., Aciego, S. M., Bourdon, B., and Kleine, T. 2015. Hf–W Chronology of the Eucrite Parent Body. *Geochimica et Cosmochimica Acta* 156: 106–21.

Treiman, A. H., Lanzirotti, A., and Xirouchakis, D. 2004. Ancient Water on Asteroid 4 Vesta: Evidence from a Quartz Veinlet in the Serra de Magé Eucrite Meteorite. *Earth and Planetary Science Letters* 219: 189–99.

Vollmer, C., Rombeck, S., Roszjar, J., Sarafian, A. R., and Klemme, S. 2020. The Brecciated Texture of Polymict Eucrites: Petrographic Investigations of Unequilibrated Meteorites from the Antarctic Yamato Collection. *Meteoritics & Planetary Science* 55: 558–74.

Warren, P. H., and Jerde, E. 1987. Composition and Origin of Nuevo Laredo Trend Eucrites. *Geochimica et Cosmochimica Acta* 51: 713–25.

Warren P. H., Jerde E. A., Migdisova L. F., and Yaroshevsky A. A. 1990. Pomozdino: An Anomalous, High-MgO/FeO, Yet REE-Rich Eucrite. Proceedings of the 20th Lunar and Planetary Science Conference. pp. 281–297.

Warren, P. H., Kallemeyn, G. W., Huber, H., Ulf-Moller, F., and Choe, W. 2009. Siderophile and Other Geochemical Constraints on Mixing Relationships among HED-Meteorite Breccias. *Geochimica et Cosmochimica Acta* 73: 5818–943.

Warren, P. H., Rubin, A. E., Isa, J., Gessler, N., Ahn, I., and Choi, B. G. 2014. Northwest Africa 5738: Multistage Fluid-Driven Secondary Alteration in an Extraordinarily Evolved Eucrite. *Geochimica et Cosmochimica Acta* 141: 199–227.

Wasson, J. T. 2013. Vesta and Extensively Melted Asteroids: Why HED Meteorites Are Probably Not from Vesta. *Earth and Planetary Science Letters* 381: 138–46.

Williams, D. A., Yingst, R. A., and Gary, W. B. 2014. Introduction: The Geologic Mapping of Vesta. *Icarus* 244: 1–12.

Yamaguchi, A. 2000. Spinels in Basaltic Eucrites: Implication for Crystallization and Metamorphic History. *Meteoritics & Planetary Sciences* 35: A174.

Yamaguchi, A., Barrat, J. A., Greenwood, R. C., Shirai, N., Okamoto, C., Setoyanagi, T., Ebihara, M., Franchi, I. A., and Bohn, M. 2009. Crustal Partial Melting on Vesta: Evidence from Highly Metamorphosed Eucrites. *Geochimica et Cosmochimica Acta* 73: 7162–82.

Yamaguchi, A., Shirai, N., Okamoto, C., and Ebihara, M. 2017. Petrogenesis of the EET 92023 Achondrite and Implications for Early Impact Events. *Meteoritics & Planetary Science* 52: 709–21.

Yamaguchi, A., Taylor, G. J., and Keil, K. 1996. Global Crustal Metamorphism of the Eucrite Parent Body. *Icarus* 124: 97–112.

Yamaguchi, A., Taylor, G. J., and Keil, K. 1997. Metamorphic History of the Eucritic Crust of 4 Vesta. *Journal of Geophysical Research* 102: 13381–6.

Zhang, A. C., Wang, R. C., Hsu, W. B., and Bartoschewitz, R. 2013. Record of S-Rich Vapors on Asteroid 4 Vesta: Sulfurization in the Northwest Africa 2339 Eucrite. *Geochimica et Cosmochimica Acta* 109: 1–13.

Zhou, Q., Yin, Q.-Z., Edward, D. Y., Li, X.-H., Wu, F.-Y., Li, Q.-L., Liu, Y., and Tang, G.-Q. 2013. SIMS Pb-Pb and U-Pb Age Determination of Eucrite Zircons at <5 Micron Scale and the First 50 Ma of the Thermal History of Vesta. *Geochimica et Cosmochimica Acta* 110: 152–75.

SUPPORTING INFORMATION

Additional supporting information may be found in the online version of this article.

Appendix S1. Additional supporting information (Fall reports and coordinates, SEM images, X-ray maps, EPMA data, Raman data) may be found in the online version of this article.